Synergistic Effect between Ultrasmall Cu(II) Oxide and CuCr 2 O 4 Spinel Nanoparticles in Selective Hydroxylation of Benzene to Phenol with Air as Oxidant

ARTICLE *in* ACS CATALYSIS · MAY 2015

Impact Factor: 9.31 · DOI: 10.1021/cs5020699

6 AUTHORS, INCLUDING:

Shankha Shubhra Acharyya
Indian Institute of Petroleum (IIP)
33 PUBLICATIONS **175** CITATIONS
SEE PROFILE

Ritesh Tiwari
University of Petroleum & Energy Studies
8 PUBLICATIONS **85** CITATIONS
SEE PROFILE

Takehiko Sasaki
The University of Tokyo
118 PUBLICATIONS **1,752** CITATIONS
SEE PROFILE

Rajaram Bal
Indian Institute of Petroleum (IIP)
69 PUBLICATIONS **681** CITATIONS
SEE PROFILE

ACS Catalysis

Research Article

pubs.acs.org/acscatalysis

Synergistic Effect between Ultrasmall Cu(II) Oxide and $CuCr_2O_4$ Spinel Nanoparticles in Selective Hydroxylation of Benzene to Phenol with Air as Oxidant

Shankha Shubhra Acharyya,[†] Shilpi Ghosh,[†] Ritesh Tiwari,[†] Chandrashekar Pendem,[†] Takehiko Sasaki,[‡] and Rajaram Bal*[,†]

[†]Catalytic Conversion & Processes Division, CSIR-Indian Institute of Petroleum, Dehradun 248005, India

[‡]Department of Complexity Science and Engineering, Graduate School of Frontier Sciences, The University of Tokyo, Kashiwanoha, Kashiwa-shi, Chiba 277-8561, Japan

Supporting Information

ABSTRACT: Phenol is an important commodity chemical, and the catalytic conversion of benzene to phenol by molecular oxygen with minimum waste production is of high significance from an academic as well as industrial point of view. We have developed a facile synthesis method for the preparation of 2−8 nm Cu(II) oxide nanoparticles supported on $CuCr_2O_4$ spinel nanoparticles (with size ∼55 nm). Detailed characterization of the material was carried out by XRD, SEM, TEM, XPS, FTIR, TGA, TPR, BET surface area, XANES, and ICP-AES methods. XRD and XPS analyses revealed that the main phase is $CuCr_2O_4$ spinel, where a small amount of CuO is dispersed on it. The catalyst was highly active for selective oxidation of benzene to phenol with air as oxidant. The influence of reaction parameters was investigated in detail. The high catalytic performance of the catalyst is due to the ultrasmall size of Cu(II) oxide nanoparticles and the strong synergy between ultrasmall Cu(II) oxide and $CuCr_2O_4$ spinel nanoparticles that plays a pivotal role in activating air to generate active oxygen species which accomplishes benzene to phenol conversion (36%) with very high selectivity (78%) in a continuous process.

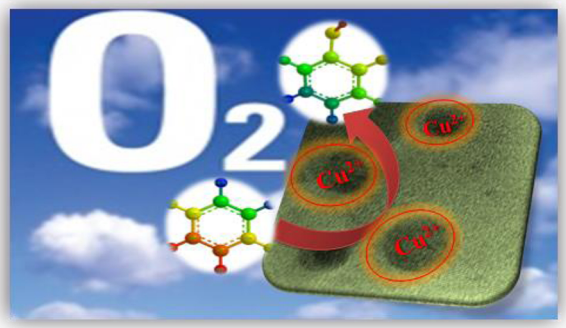

KEYWORDS: *ultrasmall Cu(II) oxide, $CuCr_2O_4$ spinel nanoparticles, benzene, phenol, air*

1. INTRODUCTION

Production of new chemical compounds by means of direct activation of C−H bonds has been a subject of potential interest.[1] Transition-metal-catalyzed hydroxylation of C−H bonds, categorized under this subject, has received considerable attention because of the industrially important alcohol or phenol products.[2,3] Despite significant development in the past few decades,[1,2] catalytic hydroxylation of C_{sp^2}−H bonds via activation of C−H bonds still remains a very challenging to researchers, as C−H bonds are thermodynamically strong and kinetically inert.[3,4] Phenol is an instance of such a type of compound, which is the major source of Bakelite and phenol resins, which are utilized in many industries over the world.[5] The industrial demand for phenol is increasing every year, and its production currently exceeds 7.2 megatons per year. Major worldwide production of phenol is carried out by a well-known three-step process, called the cumene process,[6] where the initial source is benzene. The cumene process is energy-consuming, environmentally unfavorable, and disadvantageous for practical operation, and the process also produces unnecessary by-products such as acetone and α-methylstyrene. Furthermore, the intermediate, cumene hydroperoxide, is explosive and cannot be concentrated in the final step, resulting in a very low yield of phenol. Thus, direct phenol synthesis from benzene in a one-step reaction with high benzene conversion and high phenol selectivity is most desirable from the viewpoints of an environmentally benign green process and economical efficiency. Various methods have therefore been investigated to replace it by a more benign process, which has been called one of the 10 challenges of catalysis.[7] Many researchers have come forward to overcome this difficulty and reported benzene hydroxylation reactions using different oxidants such as N_2O,[8] H_2O_2,[9] $NH_3 + O_2$,[10] air + CO,[11] molecular O_2, etc.[12] but in most cases the phenol yield is very low because phenol is more reactive toward oxidation than benzene and overoxidized products are readily formed.[13] The rapid deactivation of the catalyst by coke deposition during the gas-phase reaction is also a major concern.[14]

In light of the desirability of sustainable chemistry, catalytic oxidation of benzene using molecular oxygen as the oxidant is

Received: December 23, 2014
Revised: March 23, 2015

DOI: 10.1021/cs5020699
ACS Catal. 2015, 5, 2850−2858

of high potential interest. From a green chemistry perspective, molecular oxygen is regarded as an ideal oxidant because of its natural, inexpensive, and environmentally friendly characteristics.[15] However, catalytic aerobic oxidation of benzene via molecular oxygen activation is not an easy task, since the O_2 molecule possesses a double bond with a length of 1.208 Å and 497 kJ mol^{-1} dissociation energy.[16] In its ground state, the O_2 molecule resides in its triplet state and is reluctant to undergo formation of highly reactive oxygen radicals, hydroxyl radicals, hydroperoxides, and peroxides.[16] Although these hurdles can be overcome by using transition-metal complexes to activate both O and the C−H bond, catalytic activity, stability, and selectivity are still important issues in current research and therefore, catalytic aerobic C−H oxidation is one of the "dream reactions" from both a laboratory and an industrial point of view.[16] Recently, Shang et al. reported a 5% yield of phenol by hydroxylation of benzene by Pd−VO_x nanoparticles using molecular oxygen.[17] Very recently, Long et al. reported a phenol yield of 14% using C_3N_4−$H_5PMo_{10}V_2O_{40}$ in reductant-free aerobic oxidation of benzene.[18] In these cases, however, the yield of phenol is too poor to be scalable to an industrial level.

Several researchers have tried to synthesize phenol by direct oxidation of benzene using Cu(II)-supported catalysts.[19] Recently, we have developed nanoclusters of Cu(II) supported on a $CuCr_2O_4$ spinel nanoparticle catalytic system for the oxyamination of benzene to aniline with very high selectivity.[20] We speculated on the formation of phenol as a side product in that reaction. On the basis of the above experimental finding, we envisioned that Cu(II) oxide nanoparticles supported on $CuCr_2O_4$ spinel nanoparticles efficiently activate C_{sp^2}−H bond in benzene selectively.

Herein, we report the direct hydroxylation of benzene with a phenol yield of ∼28% over polyethylene glycol (PEG)-assisted formation of ultrasmall Cu(II) oxide nanoparticles supported on $CuCr_2O_4$ spinel nanoparticle catalyst, featuring air as the sole oxidant. We demonstrate that the catalyst is highly selective and efficient and the synergistic mechanism between supported Cu(II) oxide nanoparticles and $CuCr_2O_4$ spinel nanoparticles is detrimental factor to its high activity. To the best of our knowledge, there has been no report on benzene hydroxylation that has furnished a high yield of phenol using air as oxidant.

2. EXPERIMENTAL SECTION

2.1. Synthesis of Catalyst. Ultrasmall Cu(II) supported on $CuCr_2O_4$ spinel nanoparticle catalyst was prepared according to the protocol described in previous literature.[1] In a typical synthesis procedure, an aqueous solution of 2.25 g of $Cu(NO_3)_2{\cdot}3H_2O$ (from Sigma-Aldrich) was added to to 7.5 g of $Cr(NO_3)_3{\cdot}9H_2O$ (from Sigma-Aldrich) dissolved in 39 g of deionized water to give a clear dark blue homogeneous solution. The pH of the solution was made 8 by gradual addition of a few drops of ammonia solution. An ethanolic solution (10%) of 2.55 g of CTAB (from Sigma-Aldrich) was added dropwise followed by addition of 0.6 g of hydrazine (from Sigma-Aldrich) to the reaction mixture. The reagents were added maintaining the molar ratio Cu:Cr:CTAB:-H_2O:hydrazine = 1:2:0.75:250:1. After it was stirred, the so obtained homogeneous solution was subjected to hydrothermal treatment at 180 °C for 24 h in a Teflon-lined autoclave vessel under autogenous pressure. The autoclave was cooled until it reached room temperature. Then, the green fluffy mixture was taken out as such. Meanwhile, 0.4 g of $Cu(NO_3)_2{\cdot}3H_2O$. and 0.50 g of CTAB were dissolved in 30 mL of polyethylene glycol (PEG) with intense stirring for 2 h, and a homogeneous transparent mauve solution was obtained. After that, the mauve solution was added to the green fluffy mixture dropwise, followed by continuous stirring for 30 min. Then the whole mixture was washed several times with ethanol and dried at 100 °C for 10 h, followed by calcination at 750 °C for 6 h in air (ramped at 1 °C/min) to get black powders of Cu−Cr composites.

2.2. Reaction Setup. All catalytic experiments were carried out with a high-pressure stainless steel down-flow microreactor setup. All of the reactions were carried out using 0.2 g of the catalyst in the form of granules. The reactor zone (430 mm length, i.d. 10 mm) above the catalyst bed packed with ceramic beads served as the preheater. The reactor was placed in a temperature-controlled furnace (Autoclave Engineers, Division of Snap Tite) with a thermocouple (K-type) placed at the center of the catalyst bed to measure the reaction temperature. The feed (i.e., benzene) was passed to the catalyst surface through the reactor using a HPLC pump at a rate of 0.1 mL min^{-1}. Pressure was maintained by air, which also served as oxidant. The gas flows were adjusted by mass flow controllers (Brooks). The product was collected in a water-cooled receiver.

The reaction stream was analyzed by an online GC (Agilent), which was equipped with a flame ionization detector (FID), connected to an HP5 capillary column (30 m length, 0.28 mm i.d., 0.25 μm film thickness. column) and a thermal conductivity detector (TCD, column Porapak Q column and with an FID using a RESTEK MXT-WAX column).

3. RESULTS AND DISCUSSION

3.1. Characterization of the Catalyst. The catalyst was characterized by XRD, SEM, TEM, XPS, FTIR, TGA, TPR, BET surface area, XANES, and ICP-AES. To determine the crystallite phase of the Cu−Cr nanocomposites, we performed X-ray diffraction (XRD) analyses as shown in Figure 1. Sharp

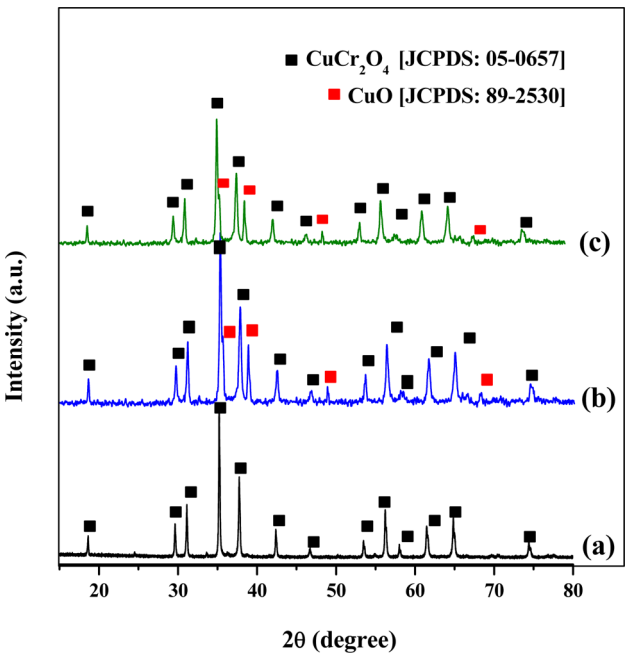

Figure 1. XRD diagram of (a) commercial $CuCr_2O_4$ spinel and our prepared (b) fresh and (c) spent catalyst.

DOI: 10.1021/cs5020699
ACS Catal. 2015, 5, 2850−2858

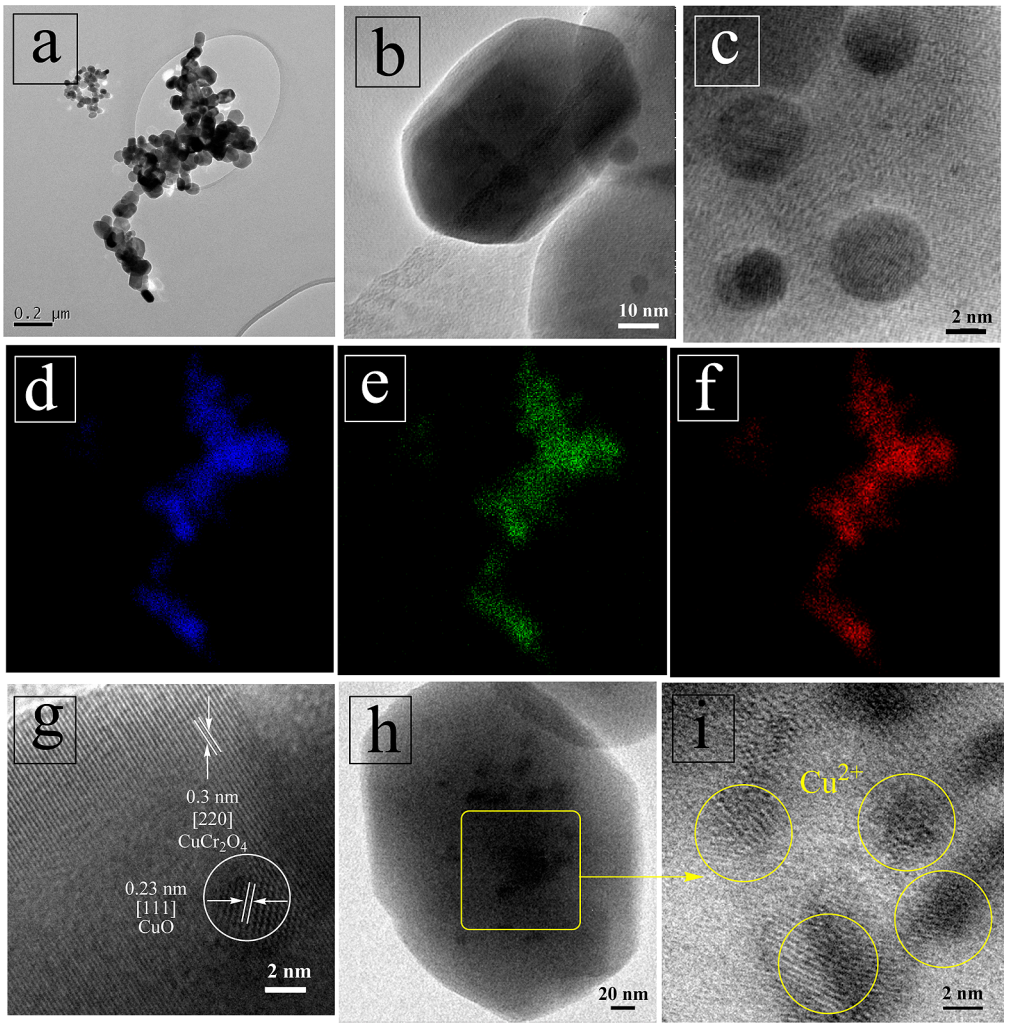

Figure 2. TEM images of (a–c) fresh catalyst at ascending resolutions, STEM-elemental mapping of (d) Cu, (e) Cr, and (f) O, (g) HRTEM of fresh catalyst, and (h, i) TEM images of spent catalyst at ascending resolutions.

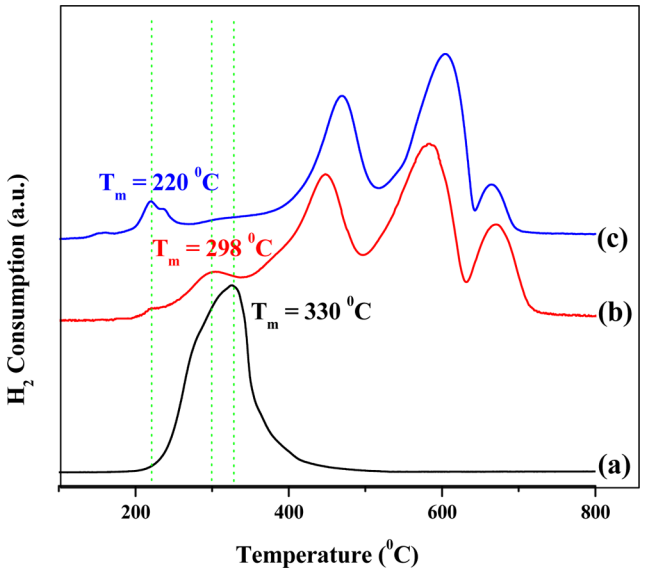

Figure 3. H_2-TPR profiles of (a) commercial CuO (CuO^{COM}), (b) nanoclusters of Cu(II) supported on $CuCr_2O_4$ spinel nanoparticles (Cu(II)/$SP^{3.5}$), and (c) ultrasmall Cu(II) supported on $CuCr_2O_4$ spinel nanoparticle catalyst Cu(II)/$SP^{PEG\text{-}3.6}$.

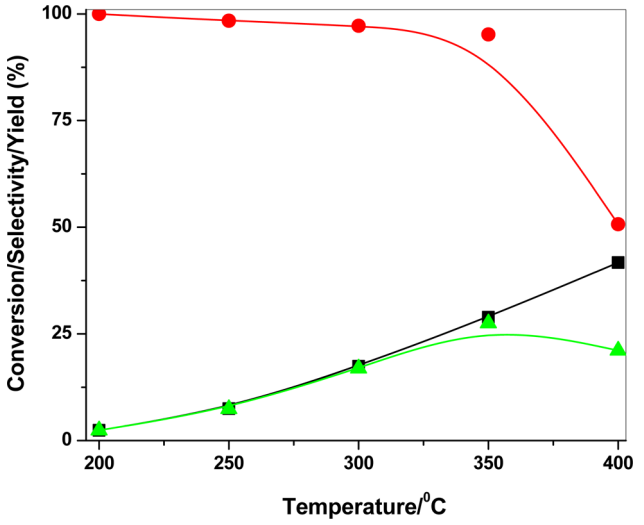

Figure 4. Effect of temperature on benzene hydroxylation: (black ■) conversion of benzene; (red ●) selectivity to phenol; (green ▲) yield of phenol. Reaction conditions: catalyst 0.2 g; pressure (air) 35 bar; benzene flow 0.1 mL min^{-1}; time 6 h.

DOI: 10.1021/cs5020699
ACS Catal. 2015, 5, 2850–2858

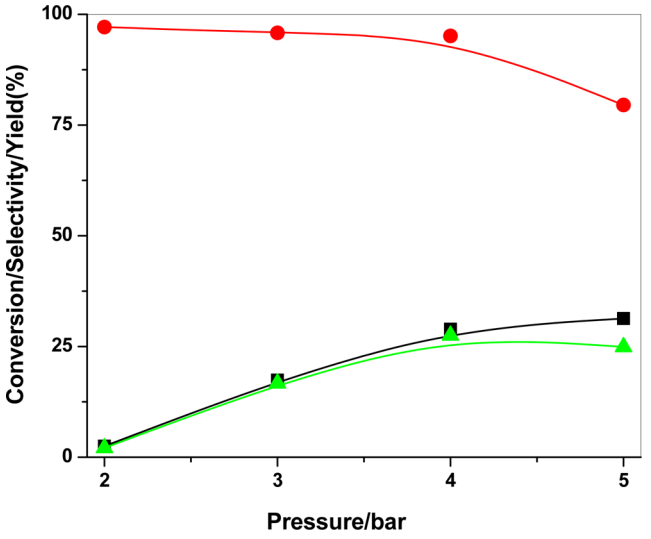

Figure 5. Effect of pressure on benzene hydroxylation: (black ■) conversion of benzene; (red ●) selectivity to phenol; (green ▲) yield of phenol. Reaction conditions: catalyst 0.2 g; temperature 350 °C; benzene flow 0.1 mL min^{-1}; time 6 h.

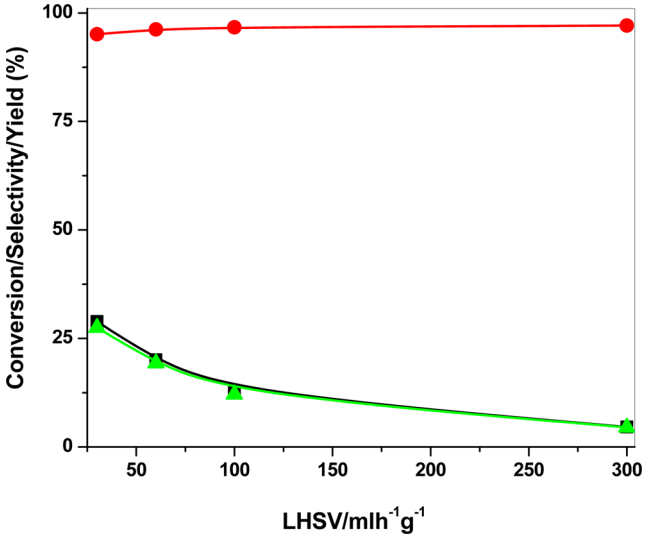

Figure 6. Effect of liquid hourly space velocity on benzene hydroxylation: (black ■) conversion of benzene; (red ●) selectivity to phenol; (green ▲) yield of phenol. Reaction conditions: catalyst 0.2 g; temperature 350 °C; benzene flow 0.1 mL min^{-1}; time 6 h.

peaks at 2θ = 18.2, 29.58, 31.07, 35.16, 37.42° correspondingly indexed as the [111], [220], [022], [311], and [113] planes of $CuCr_2O_4$ spinel (JCPDS Card No. 05-0657). In addition, XRD reflections with comparatively low peak strength due to crystalline CuO (monoclinic) were also noticed at 2θ = 35.51, 38.97, 48.68, 68.15°, etc. (JCPDS Card No. 89-2530). When the Debye–Scherrer equation was applied, the average crystallite sizes of the particles of $CuCr_2O_4$ and CuO were determined to be 28 nm (based on 2θ = 35.16°) and 6 nm (based on 2θ = 35.5°), respectively, which are actually near the size of the crystallites as seen under HRTEM imaging. Moreover, other crystalline byproducts such as $CuCrO_2$ or other phases of copper oxides were not detectable by XRD, indicating the high purity of our synthetic procedure.

XPS was utilized to detect the surface composition and the chemical state of the catalyst. The XPS binding energies (BE) of some characteristic core levels of Cu and Cr in the Cu–Cr samples have been presented (Figures S1 and S2 in the Supporting Information). The Cu 2p spectrum of the fresh sample is characterized by two spin–orbit doublets with strong satellite peaks. The so obtained Cu $2p_{3/2}$ signals fit satisfactorily to two principal peak components at ~935.3 and 933.8 eV. The BE for the Cu 2p peak was in close agreement with that of $CuCr_2O_4$, indicating that the main phase is $CuCr_2O_4$ spinel.[21] The low-energy component with Cu $2p_{3/2}$ at 933.8 eV is associated with Cu^{2+} in octahedral sites, whereas the high component at 935.3 eV is associated with Cu^{2+} in tetrahedral sites. The Cr $2p_{3/2}$ core level spectra of the $CuCr_2O_4$ fresh catalyst appeared at 576.5 eV, which shows the presence of Cr^{3+} ions in $CuCr_2O_4$ spinel.[21] Moreover, the ratio of the areas (15859.6) corresponding to the Cu $2p_{3/2}$ signal at 935.5 eV and that of the Cr $2p_{3/2}$ signal at 576.5 eV (22015.5) is 0.72, which is >0.5 (the ratio in $CuCr_2O_4$ spinel), supporting the fact that the main phase is comprised of $CuCr_2O_4$ spinel, whereas a small amount of CuO is dispersed on the spinel phase of the catalyst surface. To further investigate the surface property and to detect subtle phase information on the composite, we conducted FTIR spectroscopic analysis. Furthermore, FTIR of the spent catalyst ascertained the fact that structural deformation of the catalyst hardly took place during catalysis (Figure S3 in the Supporting Information).

The topology of the catalyst was studied by scanning electron microscopy (Figure S4 in the Supporting Information) which showed a typical sample composed of throughout uniform nanoparticles in the range of 30–60 nm. SEM images revealed that all the nanoparticles organized into spherical assemblies, owing to the structure-directing effect of the template. SEM-EDX analysis (Figure S4b in the Supporting Information) of the composite revealed that there appears a distribution of Cu, Cr, and O only, and no sort of C or Br. This observation indicated the complete removal of the structure-directing template(s). This experimental finding was further supported from TGA analysis of the uncalcined catalyst (Figure S5 in the Supporting Information). However, transmission electron microscopy (TEM) image (Figure 2a–c) revealed that some particles (i.e., $CuCr_2O_4$ spinel nanoparticles (support) are almost hexagonal (Figure 2b) with a size of 55 nm. Some spherical particles with average size 2.5 nm (Cu(II) nanoparticles) are seen to be anchored (attached) on these hexagonal particles (Figure 2b,c and Figures S6–S8 in the Supporting Information). Typically, the dispersion of Cu, Cr, and O atoms in the catalyst were also analyzed by STEM-elemental mapping (Figure 2d–f). It indicated that each of the Cu, Cr, and O species was homogeneously dispersed and this dispersion was also retained in the spent catalyst (Figure S9 in the Supporting Information). To get further information about the catalyst structure, a representative high-resolution TEM (HRTEM) image taken from a nanoparticle is shown in Figure 2g. The lattice fringes with a d spacing of 0.23 nm, corresponding to the spacing of the [111] planes of monoclinic CuO, is conveniently discriminated from that of the [211] planes of $CuCr_2O_4$ with a d spacing of 0.30 nm.[22,23] Moreover, the morphology as well as the particle size distributions (supported Cu(II)) remain almost unhindered after catalysis (as evident from TEM diagram Figure 2h,i and Figure S9). An increase in the percent of Cu loading (loading of supported Cu was varied 2.3%, 3.6%, and 7.6% and the respective catalysts are denoted as Cu(II)/$SP^{PEG-2.3}$, Cu(II)/$SP^{PEG-3.6}$, and Cu(II)/$SP^{PEG-7.6}$) changes the overall structure of the catalyst

DOI: 10.1021/cs5020699
ACS Catal. 2015, 5, 2850–2858

Table 1. Catalytic Hydroxylation of Benzene with Air as Oxidant[a]

entry	catalyst	C_B (%)[b]	S_P (%)[c]				Y_P[d] (%)	TON[e]
			Φ_{OH}	HQ	CO_2	other		
1	no catalyst	poor			>99			
2	CuO^{COM}	1.5	25	15	55	5	0.4	
3	$CuCr_2O_4{}^{COM}$	3.8	27	18	47	8	1.0	
4[f]	$CuCr_2O_4{}^{NP}$	12.5	35	22	38	5	4.4	
5[g]	$CuO-CuCr_2O_4{}^{IMP}$	14	44	17	33	6	6.2	8.6
6[h]	$Cu(II)/SP^{3.5}$	22	80	5	12	3	17.6	20.5
7[i]	$Cu(II)/SP^{PEG\text{-}2.3}$	18	84	3	8	5	15.1	26.77
8[j]	$Cu(II)/SP^{PEG\text{-}3.6}$	36	78	6	14	2	28.1	31.8
9[k]	$Cu(II)/SP^{PEG\text{-}7.6}$	44	55	15	22	8	24.2	12.9
10[l]	CuO^{NR}	2.5	28	10	57	5	0.7	

[a]Reaction conditions: catalyst 0.2 g, reaction temperature 350 °C; pressure 35 bar; benzene flow 0.1 mL min^{-1}; air flow 80 mL min^{-1}, liquid hourly space velocity (LHSV) 30 mL g^{-1} h^{-1}, time on stream 6 h, contact time (W/F) 0.114 g s mL^{-1}. Abbreviations: COM, commercial; NP, nanoparticles; SP, spinel; PEG, polyethylene glycol assisted synthesized catalyst. [b]C_B is the conversion of benzene based upon the FID-GC (GC equipped with a flame ionization detector) and is equal to 100 × (mol of benzene reacted)/(initial mol of benzene used). [c]S_p is the selectivity of products and is equal to 100 × (total mol of product(s))/(total mol of benzene consumed). [d]Y_P is the yield of phenol and is equal to (C_B × (selectivity of phenol))/100. [e]TON is the turnover number and is equal to (mol of benzene converted)/(mol of Cu in the catalyst present as supported Cu(II) on spinel). The Cu loading was estimated by inductively coupled plasma-atomic emission spectroscopy (ICP-AES). [f]$CuCr_2O_4{}^{NP}$ spinel nanoparticle catalyst. [g]$CuO-CuCr_2O_4{}^{IMP}$ is 2.9% Cu doped on commercial $CuCr_2O_4$ catalyst. [h]3.5% of Cu loading over spinel. [i]2.3% of Cu loading over spinel. [j]3.6% of Cu loading over spinel. [k]7.6% of Cu loading over spinel. [l]CuO^{NR} is supported CuO prepared hydrothermally in our process.

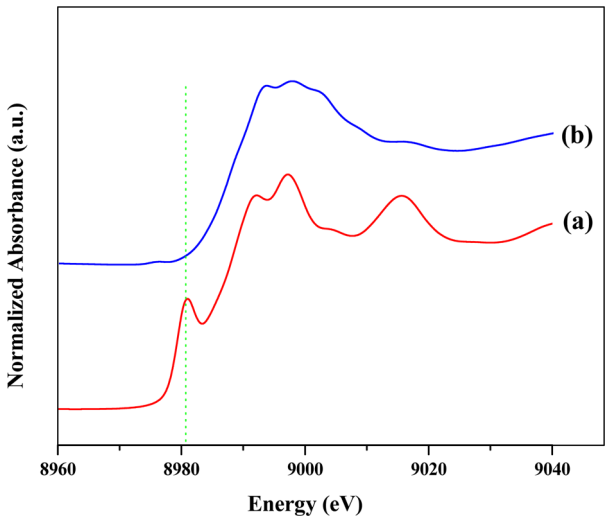

Figure 7. Cu K-edge background subtracted and normalized XANES spectra of (a) the fresh catalyst and (b) the catalyst after treatment in air, followed by a flow of benzene under optimum reaction conditions.

significantly. A comparative particle size histogram is also shown against the respective TEM diagrams (Figures S6–S8).

To obtain further insight into Cu(II)–$CuCr_2O_4$ spinel interactions and the nature as well as distribution of CuO, TPR analyses of the catalyst ($Cu(II)/SP^{PEG3.6}$) was performed (Figure 3c). The H_2-consumption peak due to Cu(II) (present as supported ultrasmall CuO) was much lower than that of commercial CuO (CuO^{COM}) with a peak maximum at about 330 °C (Figure 3a). This can be ascribed due to the fact that the supported Cu(II) species is comprised of very small Cu^{2+} nanoparticles and are easily reducible in comparison to the bulk CuO owing to dispersion effects.[24] Quantitative analysis of TPR profiles suggests that the addition of Cu(II) promoted the reducibility of the catalyst as a whole.

The corroboration of all the catalyst–characterization data led to the conclusion that the main phase of the catalyst is comprised of $CuCr_2O_4$ spinel, whereas a small amount of CuO is dispersed (as active component) on the spinel phase of the catalyst surface.

3.2. Catalytic Performance in Benzene Hydroxylation Reaction. We detected the formation of phenol as a side product when attempting to produce aniline from benzene with Cu^{2+} nanoclusters supported on $CuCr_2O_4$ spinel nanoparticles.[20] We employed this catalyst in benzene hydroxylation reactions with air as oxidant and identified phenol as the main product. Next we substituted the catalyst by $CuCr_2O_4$ spinel nanoparticle catalyst, prepared by the same process, and observed a much smaller amount of phenol formation. This serendipitous observation suggested that the key to the process is the activation of molecular oxygen (air). To our delight, PEG-assisted preparation of Cu(II) oxide nanoparticles (with average size 2.5 nm) supported on $CuCr_2O_4$ spinel nanoparticle catalyst ($Cu(II)/SP^{PEG\text{-}3.6}$) was found to be highly active in the benzene hydroxylation reaction with air as oxidant in a fixed-bed, high-pressure microreactor, and hence it was chosen as a model catalyst owing to its higher activity, convenient synthesis, and reactivity.

The temperature dependence of benzene conversion and phenol selectivity over PEG-assisted formation of Cu(II) oxide nanoparticles supported on $CuCr_2O_4$ spinel nanoparticle catalyst ($Cu(II)/SP^{PEG3.6}$) has been studied and depicted as Figure 4. The selectivity of phenol was maximum at lower temperatures (selectivity 96 and 88% at 200 and 250 °C, respectively) and decreased gradually with increasing temperature. The optimum temperature was proven to be 350 °C, over which a decrease in the yield of phenol (selectivity 55.5 at 400 °C) was observed due to the increase in the yield of CO_2, CO, etc. monotonically. When the reaction temperature was kept at 350 °C, the effect of pressure (air) on benzene hydroxylation was monitored and the results are plotted in Figure 5. The catalyst did not show any activity at atmospheric pressure. High pressure boosts the conversion of benzene. A pressure of 35 bar was proven to be optimum, since under this reaction condition, a maximum phenol yield (yield of 28%) was observed. The yields of both CO_2 and CO increased

DOI: 10.1021/cs5020699
ACS Catal. 2015, 5, 2850–2858

Scheme 1. Plausible Mechanism for the Formation of Phenol over Ultrasmall Cu(II) Supported on $CuCr_2O_4$ Spinel Nanoparticle Catalyst[19d]

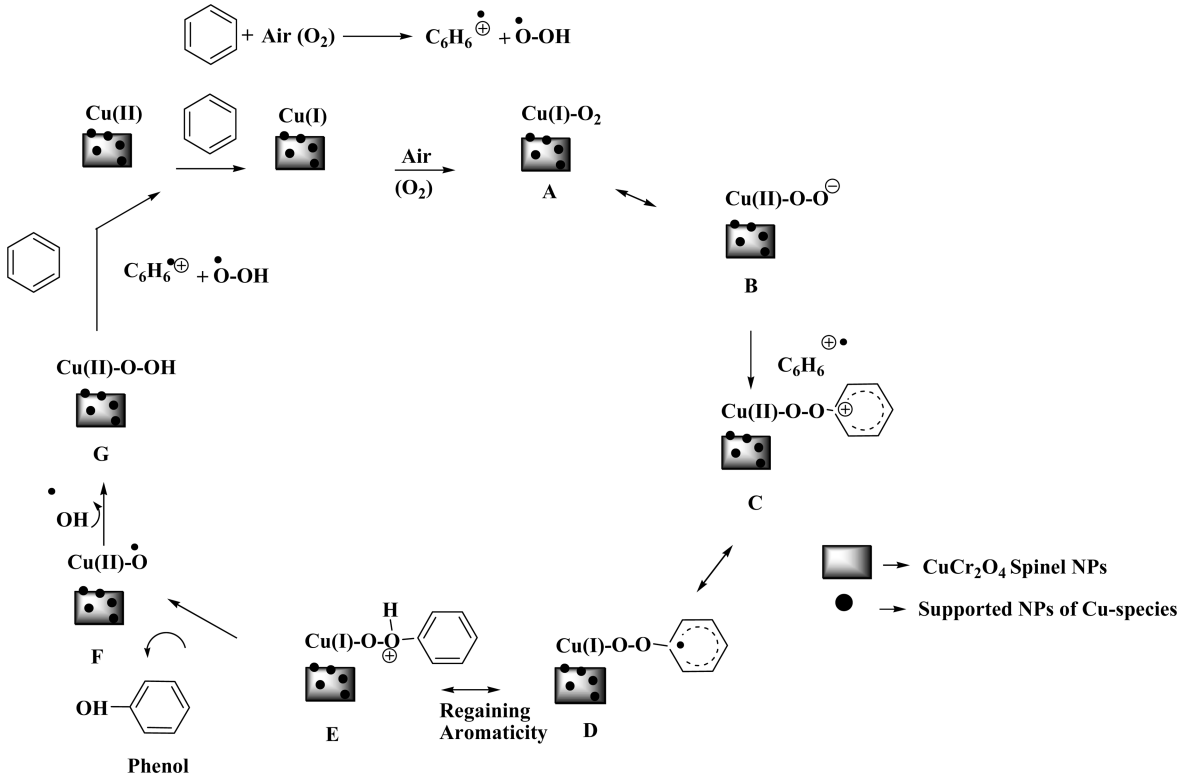

monotonically with a further increase in air pressure. This phenomenon can be attributed to the fact that the produced phenol molecules undergo overoxidation with the excess oxygen (air) supplied. The yield of phenol is largely dependent on the contact time (contact time; W/F is inversely proportional to LHSV). The dependence of benzene conversion and phenol selectivity has been plotted (Figure 6). The selectivity of phenol sharply increased with the increment of LHSV (selectivity 78%, 80%, 82%, and 86% at LHSV 30, 60, 100, and 300 mL h^{-1} g^{-1}, respectively). The increment of LHSV actually indicates that the reactants get less time to stay in contact with the catalyst surface. When the contact time is increased (W/F; i.e., at low LHSV), although the conversion of benzene increased, the selectivity of phenol decreased linearly.

A blank reaction (without using any catalyst) was performed. CO_2 was detected as the sole product, owing to auto-oxidation of benzene (entry 1, Table 1). This indicated the fact that oxygen species adsorbed on the catalyst were mainly responsible for the phenol formation, rather than gaseous O_2, which contributes to the deep oxidation of benzene to CO_2 and CO. Notably, when the benzene hydroxylation reaction was carried out using commercial CuO (CuO^{COM}; entry 2, Table1), a poor yield of phenol was obtained. When commercial spinel ($CuCr_2O_4^{COM}$, entry 3, Table1), was used as catalyst, initially formation of a low yield of phenol was observed, but the catalyst became deactivated with time, due to the leaching of Cu^{2+} species from the spinel framework (as confirmed by ICP-AES). Moreover, these catalysts lack good catalytic activity due to their irregular shapes and nonuniform sizes. These results indicate that morphology of the catalyst as well as the nature of Cu^{2+} species play an important role in affecting the catalytic activity. We also introduced nanoclusters of Cu(II) supported on nanocrystalline Cr_2O_3 as a catalyst in this reaction and observed that the catalyst was proven to be active for a short span of time, probably due to sintering of CuO nanoparticles. To rule out the possibility of leaching and sintering processes acquainted with the above catalytic systems, we applied our previously reported[9c] $CuCr_2O_4$ spinel nanoparticles catalyst ($CuCr_2O_4^{NP}$; entry 4, Table1). We noticed that, although phenol formation with considerable yield was possible, the formation of phenol was noticed after a comparatively long time (4 h). Moreover, although greater conversion of benzene was noticed with time (7 h), the selectivity of phenol decreased due to the formation of side products. This experimental finding can be attributed to the fact that probably Cu(II) species in the spinel framework are necessary to activate the aromatic C−H bond, whereas Cr(III) oxide is not involved in the reaction but stabilizes the copper ion(s) against aggregation under the reaction conditions.[21a] Moreover, the Cu(II) species in the spinel framework were hard to reduce by benzene molecules; thereby formation of phenol on the catalyst surface was inhibited due to the need for a suitable redox system.[9c,d] In our effort to enhance the catalytic activity of the catalytic system, we incorporated some extra CuO (commercial) to $CuCr_2O_4$ spinel nanoparticles catalyst by means of an impregnation method in an attempt to improve the catalytic system ($CuO-CuCr_2O_4^{IMP}$; entry 5, Table1). We observed that within 3 h the catalyst began to perform in the benzene hydroxylation reaction; however, after 4 h, the catalyst started to be deactivated due to massive leaching of extra Cu^{2+} doped on $CuCr_2O_4$ spinel. From these experimental findings it can be inferred that a supported Cu(II) species on a spinel framework is necessary for the generation of a suitable redox system to facilitate the Cu(II) ↔ Cu(I) path, thereby rendering phenol formation by direct oxidation of benzene. To prove this

DOI: 10.1021/cs5020699
ACS Catal. 2015, 5, 2850−2858

hypothesis, we introduced nanoclusters of Cu(II) supported on $CuCr_2O_4$ spinel nanoparticles prepared hydrothermally (Cu-(II)/SP)$^{3.5}$, following the protocols described in our previous report.[20] We noticed 22% benzene conversion with a phenol selectivity of 75% (entry 6, Table 1). However, we obtained a better result when we prepared ultrasmall Cu(II) oxide nanoparticles supported on $CuCr_2O_4$ spinel nanoparticle catalyst, modifying the previous method (Cu(II)/SP$^{PEG\text{-}3.6}$, entry 8, Table1). Furthermore, we prepared Cu(II) oxide nanorods hydrothermally (CuO^{NR}; entry 10, Table 1) using CTAB and applied it as a catalyst, maintaining all the optimum conditions. We noticed very low conversion of benzene with 28% selectivity to phenol. From all these observations we can tentatively suggest that, although benzene molecules become activated on the $CuCr_2O_4$ spinel surface, producing phenol with high yield consistently maintaining the catalytic system unhindered solely depends on the present catalytic system, where ultrasmall cationic Cu(II) species are located at the metal−support interface and serve as "chemical glue" to bind the species to the support. Moreover, this chemical glue is responsible for the synergy displayed between the ultrasmall Cu(II) species and the $CuCr_2O_4$ spinel surface. Furthermore, it can also be suggested that the crucial effect of the latter synthesis method is demonstrated by its strikingly superior activity in comparison to the previously reported Cu(II) nanoclusters supported on $CuCr_2O_4$ spinel nanoparticles, in spite of the fact that these two systems have the same chemical composition, the same active metal as well as support, and almost the same metal loading and BET surface areas (65 and 66 $m^2\ g^{-1}$, respectively). Such a unique nanostructure benefits the structural stability of the catalyst.

Although the mechanism of the formation of supported ultrasmall Cu(II) oxide nanoparticles is not very clear, we believe that the modifiers used in the preparation of the catalyst play an important role in the generation of the active component (here Cu^{2+})−support synergistic interaction in the catalyst. This hypothesis was further proved from a comparative study of their TPR analyses (Figure 3). There were two types of Cu(II) species present in both catalysts (i.e. nanoclusters of Cu(II) supported on $CuCr_2O_4$ spinel nanoparticles (Cu(II)/SP) and ultrasmall Cu(II) supported on $CuCr_2O_4$ spinel nanoparticle catalyst (Cu(II)/SP$^{PEG\text{-}3.6}$), which were reduced at 150−450 °C (due to supported Cu(II) species) and 450−800 °C (three peaks due to Cu(II) species in spinel), respectively. The former Cu(II) species present in both catalysts were reduced at a temperature lower than that for commercial CuO (CuO^{COM}; Figure 3a), which is reduced at 330 °C; moreover, the Cu(II) species in the present catalyst (Cu(II)/SP$^{PEG3.6}$) is reduced at a temperature comparatively lower than that for our previously reported catalyst (Cu(II)/SP$^{3.5}$). Taking into account the general dependence of T_m (temperature at maximum reduction point) on the particle size, i.e. smaller particles are expected to be reduced at lower temperature,[24] we can clearly state that the Cu(II) oxide in the present catalyst (Cu(II)/SP$^{PEG3.6}$) is much smaller and is highly dispersed on the $CuCr_2O_4$ spinel phase. Furthermore, this TPR analysis also demonstrates indirectly that Cu(II) species supported on $CuCr_2O_4$ spinel nanoparticles (in both Cu(II)/SP$^{PEG3.6}$ and Cu(II)/SP$^{3.5}$) are greatly superior (comparatively much easily reducible) in comparison to $CuCr_2O_4$ spinel nanoparticle (containing single-phased spinel) catalyst. These results are consistent with the experimental findings (Table 1), which demonstrate the fact that stable dispersed ultrasmall Cu(II)−NPs with a more accessible catalytic surface can be particularly effective in benzene hydroxylation. The synergistic effect between Cu(II) NPs and $CuCr_2O_4$ spinel plays a critical role in the formation of phenol and the support $CuCr_2O_4$, not only stopping coalescence and agglomeration of the Cu(II) nanoparticles but also supporting phenol formation. The above rationale was also followed in the experimental findings, i.e. the reactivity order of the catalysts toward benzene hydroxylation: ultrasmall Cu(II) supported on $CuCr_2O_4$ spinel nanoparticles (size of Cu(II) species 2−8 nm, i.e. Cu(II)/SP$^{PEG3.6}$) > Cu(II) nanoclusters supported on $CuCr_2O_4$ spinel nanoparticles (size of Cu(II) species 10−18 nm, i.e. Cu(II)/SP$^{3.5}$) > $CuCr_2O_4$ spinel nanoparticles (size of Cu(II) species 25−55 nm).

To further elucidate the role of supported nanoparticles in the reaction, we studied the size effect of supported Cu(II) nanoparticles (on $CuCr_2O_4$ spinel). To this end, Cu(II) NPs with average sizes ranging from 2.5 to 4.5 to 30 nm were examined under similar conditions (i.e., catalyst 0.2 g, reaction temperature 350 °C, pressure 35 bar, benzene flow 0.1 mL/min, air flow 80 mL/min, LHSV 30 mlL $g^{-1}\ h^{-1}$, TOS 6 h, and contact time (W/F) 0.114 g s mL^{-1}; Table 1). A significant difference was noted in the activities of the first two catalysts at 2.4 and 3.6 wt % of copper loading on spinel (entries 7 and 8, Table 1). When the average size of the Cu(II) NPs increased to 30 nm (3.6 wt % of copper loading on spinel), however, the reaction rate decreased drastically (entry 9, Table 1). This can be explained by the fact that further increasing the Cu content to 7.6 wt % (on spinel), the slight aggregation of Cu nanoparticles on the surface of $CuCr_2O_4$ result in a decrease in the number of active sites on the surface of the catalyst. These observations substantiated that the surface area and morphology of the samples are critical to the adsorption and activation of molecular oxygen.

3.3. Benzene Hydroxylation Mechanism. To probe the reaction mechanism, several control experiments were carried out. Phenol was detected as the main product. Quinol, biphenyl, and CO_2 were detected as the main side products. Very small amounts of naphthalene, β-naphthol, and CO were detected (as confirmed from GCMS results, Figure S11−S16 in Supporting Information). When the reaction was performed under a N_2 atmosphere, no phenol was detected. Moreover, biphenyl was not detected under that atmosphere, underscoring the participation of dioxygen in the reaction. It is a well-known phenomenom that the activation of molecular oxygen occurs by transferring charge density from metal to the vacant π^* molecular orbital of adsorbed O_2.[25] It is generally believed that molecular oxygen (air) dissociates on Cu(I) oxide,[26,27] which is produced concomitantly and thereby generates active oxygen species,[26] although the detailed reaction mechanism is still unknown. To find the probable mechanism of benzene hydroxylation during catalysis, the catalyst was kept for several hours with all the reaction conditions unaffected; after that, the flow of air was stopped and the catalyst was kept under a continuous flow of benzene. During this period, the pressure was maintained by N_2. Then the catalyst was recovered and was subjected to XANES analysis. The Cu K-edge XANES spectra of the fresh catalyst displayed absorption edge positions at 8982 and 8987 eV, indicative of Cu^{2+} species in the catalyst (supported Cu(II), which served as the active component). However, after treatment in air, followed by benzene flow at high temperature and pressure, this specific peak disappears (Figure 7); interestingly, this change does not occur if the catalyst is kept under benzene flow only. This experimental

DOI: 10.1021/cs5020699
ACS Catal. 2015, 5, 2850−2858

finding led to the conclusion that while oxygen adsorption oxidizes the Cu(I) ions to Cu(II) ions, the reverse path is facilitated by reduction of Cu(II) ions caused by benzene molecules.

The benzene hydroxylation reaction mechanism over ultrasmall Cu(II) oxide supported on $CuCr_2O_4$ spinel nanoparticles can be postulated (Scheme 1).[26] Cr(III) (in the catalyst) is believed to act as a textural promoter that prevents sintering of the Cu(II) oxide and, hence, the surface area of the catalyst is preserved during catalysis.[28] Benzene reduces the supported Cu(II) species to Cu(I) species A, which transforms into its canonical form B; meanwhile, benzene produces benzene radical cation ($C_6H_6^{\bullet+}$) and peroxide radical ($HOO^{\bullet}$). In the next step, $C_6H_6^{\bullet+}$ radical reacts with B to produce complex C, which can be transformed into its canonical form D. D eliminates a proton to restore the aromaticity (E). Then E dissociates into Cu(II) oxide species F and phenol. F interacts with concomitantly formed $^{\bullet}OH$ radical to form G. This cycle is closed by reducing G back to a Cu(I) species by a benzene molecule with the formation of benzene radical cation, which can re-enter the cycle.

4. CONCLUSIONS

In summary, we have introduced a polyethylene glycol assisted method for the synthesis of ultrasmall Cu(II) oxide nanoparticles supported on $CuCr_2O_4$ spinel nanoparticles. We clearly demonstrated the importance of the morphology-controlled ultrasmall Cu(II)−spinel interaction, which has a great influence on the benzene hydroxylation reaction. The catalyst displayed excellent catalytic performance in the sustainable hydroxylation of benzene with air as oxidant, achieving high efficiency in terms of activity, selectivity, and stability. The attractive features of the catalyst are very promising, as it may serve as a potential alternative to the existing cumene process.

■ ASSOCIATED CONTENT

Ⓢ Supporting Information

The following file is available free of charge on the ACS Publications website at DOI: 10.1021/cs5020699.

Details of the characterization techniques and preparations and characterization data (PDF)

■ AUTHOR INFORMATION

Corresponding Author

*R.B.: tel, +91 135 2525917; fax, +91 135 2660202; e-mail, raja@iip.res.in.

Notes

The authors declare no competing financial interest.

■ ACKNOWLEDGMENTS

S.S.A. thanks the CSIR and S.G. thanks the UGC of India for a fellowship. The Director of the CSIR-IIP is acknowledged for his help and encouragement. The authors thank the Analytical Science Division, CSIR-Indian Institute of Petroleum, for analytical services. R.B. thanks the CSIR, New Delhi, India, for financial support in the form of the 12 FYP Project (CSC-0125, CSC- 0117). The XAFS measurements were performed at KEK-IMSS-PF with the approval of the Photon Factory Advisory Committee (project 2013G210).

■ REFERENCES

(1) (a) Mkhalid, I. A. I.; Barnard, J. H.; Marder, T. B.; Murphy, J. M.; Hartwig, J. F. *Chem. Rev.* **2010**, *110*, 890−931. (b) Ackermann, L.; Vicente, R.; Kapdi, A. R. *Angew. Chem., Int. Ed.* **2009**, *48*, 9792−9826.

(2) (a) Bigi, M. A.; Reed, S. A.; White, M. C. *J. Am. Chem. Soc.* **2012**, *134*, 9721−9726. (b) Kamata, K.; Yonehara, K.; Nakagawa, Y.; Uehara, K.; Mizuno, N. *Nat. Chem.* **2010**, *2*, 478−483.

(3) Yan, Y.; Feng, P.; Zheng, Q. Z.; Liang, Y. F.; Lu, J. F.; Cui, Y.; Jiao, N. *Angew. Chem., Int. Ed.* **2013**, *52*, 5827−5831.

(4) (a) Goldman, A. S.; Goldberg, K. I. *Activation and Functionalization of C-H Bonds*; American Chemical Society: Washington, DC, 2004, ACS Symposium Series *885*, pp 1−45. (b) Balcells, D.; Clot, E.; Eisenstein, O. *Chem. Rev.* **2010**, *110*, 749−823. (c) Gunay, A.; Theopold, K. H. *Chem. Rev.* **2010**, *110*, 1060−1081.

(5) Fiege, H.; Voges, H. W.; Hamamoto, T.; Umemura, S.; Iwata, T.; Miki, H.; Fujita, Y.; Buysch, H. J.; Garbe, D.; Paulus, W. *Ullmann's Encyclopedia of Industrial Chemistry*; Wiley-VCH: Weinheim, Germany, 2000; Vol. *26* (phenol derivatives), pp 521−576.

(6) Tada, M.; Bal, R.; Sasaki, T.; Uemura, Y.; Inada, Y.; Tanaka, S.; Nomura, M.; Iwasawa, Y. *J. Phys. Chem. C* **2007**, *111*, 10095−10104.

(7) (a) Löcke, B.; Narayana, K. V.; Martin, A.; Jähnisch, K. *Adv. Synth. Catal.* **2004**, *346*, 1407−1424. (b) Cornils, B.; Herrmann, W. A. *J. Catal.* **2003**, *216*, 23−31.

(8) Xin, H.; Koekkoek, A.; Yang, Q.; van Santen, R. A.; Li, C.; Hensen, E. J. M. *Chem. Commun.* **2009**, 7590−7592.

(9) (a) Tanev, P. T.; Chibwe, M.; Pinnavaia, T. J. *Nature* **1994**, *368*, 321−323. (b) Borah, P.; Ma, X.; Nguyen, K. T.; Zhao, Y. *Angew. Chem., Int. Ed.* **2012**, *51*, 7756−7761. (c) Acharyya, S. S.; Ghosh, S.; Adak, S.; Sasaki, T.; Bal, R. *Catal. Sci. Technol.* **2014**, *4*, 4232−4241. (d) Acharyya, S. S.; Ghosh, S.; Bal, R. *ACS Appl. Mater. Interfaces* **2014**, *6*, 14451−14459.

(10) (a) Bal, R.; Tada, M.; Sasaki, T.; Iwasawa, Y. *Angew. Chem., Int. Ed.* **2006**, *45*, 448−452. (b) Wang, L.; Yamamoto, S.; Malwadkar, S.; Nagamatsu, S.; Sasaki, T.; Hayashizaki, K.; Tada, M.; Iwasawa, Y. *ChemCatChem* **2013**, *5*, 2203−2206.

(11) Tani, M.; Sakamoto, T.; Mita, S.; Sakaguchi, S.; Ishii, Y. *Angew. Chem., Int. Ed.* **2005**, *44*, 2586−2588.

(12) Shibata, Y.; Hamada, R.; Ueda, T.; Ichihashi, Y.; Nishiyama, S.; Tsuruya, S. *Ind. Eng. Chem. Res.* **2005**, *44*, 8765−8772.

(13) Sheldon, R. A.; Kochi, J. K. *Metal-Catalyzed Oxidations of Organic Compounds*; Academic Press: New York, 1981; pp 329−333.

(14) Panov, G. I.; Kharitonov, A. S.; Sobolev, V. I. *Appl. Catal., A* **1993**, *98*, 33−43.

(15) Cai, S.; Rong, H.; Yu, X.; Liu, X.; Wang, D.; He, W.; Li, Y. *ACS Catal.* **2013**, *3*, 478−486.

(16) Roduner, E.; Kaim, W.; Sarkar, B.; Urlacher, V. B.; Pleiss, J.; Gläser, R.; Einicke, W. D.; Sprenger, G. A.; Beifuß, U.; Klemm, E.; Liebner, C.; Hieronymus, H.; Hsu, S. F.; Plietker, B.; Laschat, S. *ChemCatChem* **2013**, *5*, 82−112.

(17) Shang, S.; Yang, H.; Li, J.; Chen, B.; Lv, Y.; Gao, S. *ChemPlusChem* **2014**, *79*, 680−683.

(18) Long, Z.; Zhou, Y.; Chen, G.; Ge, W.; Wang, J. *Sci. Rep.* **2014**, *4* (3651), 1−5.

(19) (a) Hamada, R.; Shibata, Y.; Nishiyama, S.; Tsuruya, S. *Phys. Chem. Chem. Phys.* **2003**, *5*, 956−965. (b) Kitamura, T.; Kanzaki, H.; Hamada, R.; Nishiyama, S.; Tsuruya, S. *Can. J. Chem.* **2004**, *82*, 1597−1605. (c) Archipov, T.; Santra, S.; Ene, A. B.; Stoll, H.; Rauhut, G.; Roduner, E. *J. Phys. Chem. C* **2009**, *113*, 4107−4116. (d) Ene, A. B.; Archipov, T.; Roduner, E. *J. Phys. Chem. C* **2011**, *115*, 3688−3694.

(20) Acharyya, S. S.; Ghosh, S.; Bal, R. *Chem. Commun.* **2014**, *50*, 13311−13314.

(21) (a) Pantaleo, G.; Liotta, L. F.; Venezia, A. M.; Deganello, G.; Ezzo, E. M.; El Kherbawi, M. A.; Atia, H. *Mater. Chem. Phys.* **2009**, *114*, 604−611. (b) Severino, F.; Brito, J. L.; Laine, J.; Fierro, J. L. G.; L'opez Agudoy, A. *J. Catal.* **1998**, *177*, 82−95.

(22) Kawamoto, A. M.; Pardini, L. C.; Rezende, L. C. *Aerosp. Sci. Technol.* **2004**, *8*, 591−598.

DOI: 10.1021/cs5020699
ACS Catal. 2015, 5, 2850−2858

(23) Chary, K. V. R.; Sagar, G. V.; Naresh, D.; Seela, K. K.; Sridhar, B. *J. Phys. Chem. B* **2005**, *109*, 9437.
(24) Huo, C.; Ouyang, J.; Yang, H. *Sci. Rep.* **2014**, *4* (3682), 1−9.
(25) Ghosh, S.; Acharyya, S. S.; Tiwari, R.; Sarkar, B.; Singha, R. K.; Pendem, C.; Sasaki, T.; Bal, R. *ACS Catal.* **2014**, *4*, 2169−2174.
(26) (a) Ene, A. B.; Archipov, T.; Roduner, E. *J. Phys. Chem. C* **2011**, *115*, 3688−3694. (b) Kromer, A.; Roduner, E. *ChemPlusChem* **2013**, *78*, 268−273. (c) Tabler, A.; Häusser, A.; Roduner, E. *J. Mol. Catal. A: Chem.* **2013**, *379*, 139−145.
(27) Liu, P.; Hensen, E. J. M. *J. Am. Chem. Soc.* **2013**, *135*, 14032−14035.
(28) Edwards, M. A.; Whittle, D. M.; Rhodes, C.; Ward, A. M.; Rohan, D.; Shannon, M. D.; Hutchings, G. J.; Kiely, C. J. *Phys. Chem. Chem. Phys.* **2002**, *4*, 3902−3908.

DOI: 10.1021/cs5020699
ACS Catal. 2015, 5, 2850−2858